Citation: Cell Death and Disease (2012) 3, e390; doi:10.1038/cddis.2012.120

www.nature.com/cddis

AIF-mediated caspase-independent necroptosis requires ATM and DNA-PK-induced histone H2AX Ser139 phosphorylation

M Baritaud[1,2,3], L Cabon[1,2,3], L Delavallée[1,2,3], P Galán-Malo[1,2,3], M-E Gilles[1,2,3], M-N Brunelle-Navas[1,2,3] and SA Susin*[,1,2,3]

The alkylating DNA-damage agent *N*-methyl-*N*′-nitro-*N*-nitrosoguanidine (MNNG) induces a form of caspase-independent necroptosis implicating the mitochondrial flavoprotein apoptosis-inducing factor (AIF). Following the activation of PARP-1 (poly(ADP-ribose) polymerase-1), calpains, BID (BH3 interacting domain death agonist), and BAX (Bcl-2-associated X protein), the apoptogenic form of AIF (tAIF) is translocated to the nucleus where, associated with Ser139-phosphorylated histone H2AX (γH2AX), it creates a DNA-degrading complex that provokes chromatinolysis and cell death by necroptosis. The generation of γH2AX is crucial for this form of cell death, as mutation of H2AX Ser139 to Ala or genetic ablation of H2AX abolish both chromatinolysis and necroptosis. On the contrary, reintroduction of H2AX-wt or the phosphomimetic H2AX mutant (H2AX-S139E) into *H2AX*$^{-/-}$ cells resensitizes to MNNG-triggered necroptosis. Employing a pharmacological approach and gene knockout cells, we also demonstrate in this paper that the phosphatidylinositol-3-OH kinase-related kinases (PIKKs) ATM (ataxia telangiectasia mutated) and DNA-dependent protein kinase (DNA-PK) mediate γH2AX generation and, consequently, MNNG-induced necroptosis. By contrast, H2AX phosphorylation is not regulated by ATR or other H2AX-related kinases, such as JNK. Interestingly, ATM and DNA-PK phosphorylate H2AX at Ser139 in a synergistic manner with different kinetics of activation. Early after MNNG treatment, ATM generates γH2AX. Further, DNA-PK contributes to H2AX Ser139 phosphorylation. In revealing the pivotal role of PIKKs in MNNG-induced cell death, our data uncover a milestone in the mechanisms regulating AIF-mediated caspase-independent necroptosis.

Cell Death and Disease (2012) **3,** e390; doi:10.1038/cddis.2012.120; published online 13 September 2012
Subject Category: Cancer

Originally considered as an uncontrolled passive event, some forms of necrosis have recently been recognized as programmed modes of cell death.[1,2] Programmed necrosis can be triggered by default when the classical apoptotic enzymes, caspases, are inhibited. More interestingly, it can also occur under multiple pathological conditions, including cancer, ischemia-reperfusion injury, neurodegeneration, cerulein-induced acute pancreatitis, retinal detachment-induced photoreceptor death, Crohn's disease, systemic inflammatory response syndrome, and viral infection.[3] Thus, the physiopathological relevance of programmed necrosis contributes to the increasing interest in unraveling the molecular determinants that control this newly defined mode of programmed cell death (PCD).

One of the most studied forms of programmed necrosis is necroptosis, which includes, at least two different forms of PCD.[1] The first necroptotic pathway described is the PCD process induced by tumor necrosis factor (TNF).[1,2] Stimulation of TNF receptor 1 by TNFα leads to the formation of a complex in the cellular membrane that includes TRADD (tumor necrosis factor receptor type 1-associated death domain), TRAF2 (TNF receptor-associated factor 2), RIP1 (receptor interacting protein-1), and cIAP1 (baculoviral IAP repeat-containing protein 1). Under apoptosis-deficient conditions, these components dissociate and RIP1 is released into the cytosol. Cytoplasmic RIP1 interacts with receptor interacting protein-3 (RIP3) to form a complex triggering the necroptotic PCD pathway.[2] As demonstrated by the use of Necrostatin-1 (Nec-1), a small molecule identified in a chemical library screen as a potent inhibitor of the RIP1 kinase activity, the formation of this complex requires the phosphorylating properties of RIP1.[4] Downstream of RIP1 and RIP3, three proteins act as lethal effectors in TNF-induced necroptosis: mixed lineage kinase domain-like

[1]INSERM U872, Programmed cell death and physiopathology of tumor cells. Team n° 19, Centre de Recherche des Cordeliers, Paris, France; [2]Université Pierre et Marie Curie-Sorbonne Universités, UMRS 872, Paris, France and [3]Université Paris Descartes, UMRS 872, Paris, France
*Corresponding author: SA Susin, Centre de Recherche des Cordeliers. 15, rue de l'Ecole de Médecine, 75006 Paris, France. Tel: +33 1 44279070; Fax: +33 1 44279036; E-mail: santos.susin@crc.jussieu.fr
Keywords: AIF; ATM; DNA-PK; H2AX; necroptosis
Abbreviations: AIF, apoptosis-inducing factor; ATM, ataxia telangiectasia mutated; ATR, ATM- and Rad-3 related; BAX, Bcl-2-associated X protein; BCL-2, B-cell lymphoma 2; BID, BH3 interacting domain death agonist; CAD, caspase-activated DNase; CypA, cyclophilin A; DSBs, double-strand breaks; DNA-PK, DNA dependent protein kinase; FCS, fetal calf serum; JNK1, c-Jun NH2-terminal kinase 1; Q-VD.OPh, Gln-Val-Asp(non-Omethylated)-Oph; MEFs, murine embryonic fibroblasts; MNNG, N-methyl-N′-nitro-N-nitrosoguanidine; Nec-1, 5-(indol-3-ylmethyl)-(2-thio-3-methyl)hydantoin, Necrostatin-1; MST1, mammalian STE20-like kinase 1; PARP-1, poly(ADP-ribose) polymerase-1; PCD, programmed cell death; PIKKs, phosphatidylinositol-3-OH kinase-related kinases; RIP1, receptor interacting protein-1; RIP3, receptor interacting protein-3; TNF, tumor necrosis factor
Received 22.5.12; revised 2.7.12; accepted 12.7.12; Edited by H-U Simon

protein, phosphoglycerate mutase family member 5, and the fission mediator Drp1 (dynamin-related protein 1).[5,6] Alkylating DNA-damage-mediated caspase-independent programmed necrosis is the second necroptotic pathway described to date. Considering RIP1 kinase dependency as a hallmark of this form of death, we have recently shown that high doses of the alkylating DNA-damaging agent *N*-methyl-*N*′-nitro-*N*-nitrosoguanidine (MNNG) trigger necroptosis. Indeed, both genetic ablation of RIP1 and its pharmacological inhibition by Nec-1 prevent MNNG-induced caspase-independent PCD.[7–9]

MNNG acts by covalently modifying bases in DNA. The relevant DNA damage induced by this modification causes both the disproportionate activation of poly(ADP-ribose) polymerase-1 (PARP-1) and the phosphorylation of histone H2AX at Ser139 (γH2AX).[10–12] In mouse embryonic fibroblasts (MEFs), hyper-activated PARP-1 governs the sequential activation of the calpain Cys proteases and the proapoptotic B-cell lymphoma 2 (BCL-2) family members BID (BH3 interacting domain death agonist) and BAX (Bcl-2-associated X protein).[9,10] Once activated, BAX triggers a mitochondrial damage that, in cooperation with calpains, leads to the generation and release of the proapoptotic protein tAIF, which is the truncated form of the mitochondrial oxydoreductase apoptosis-inducing factor (AIF).[13] Once in the cytosol, this caspase-independent effector relocalizes to the nuclear compartment where, in cooperation with γH2AX and cyclophilin A (CypA), it provokes DNA degradation and PCD.[11,12] In fact, by providing a strategic bridge between tAIF and CypA, γH2AX becomes essential for the lethal DNA-degrading activity characteristic of AIF-mediated necroptosis.

H2AX, a member of the histone H2A family,[14] is characterized by a phosphorylable SQE motif in its C-terminal tail. The generation of double-strand breaks (DSBs) is related to the phosphorylation of the H2AX C-terminal tail at Ser139 that yields γH2AX. Once generated, γH2AX accumulates at the sites of DSBs,[15,16] where it is thought to restructure chromatin and assist in the recruitment/retention of DNA repair and signaling factors.[14,17] Even if the function of H2AX is mainly associated with DNA-damage repair and DNA packaging,[16] this histone is also key in PCD.[18,19] In UV-induced caspase-dependent cell death, it seems that γH2AX alters chromatin conformation to increase the accessibility of nucleosomal DNA to the DNase CAD (caspase-activated DNase). In this particular caspase-dependent PCD system, H2AX phosphorylation at Ser139 is mediated by c-Jun NH2-terminal kinase 1 (JNK1), a member of the mitogen-activated protein kinase group.[19] In other types of caspase-dependent PCD, H2AX is phosphorylated either by the caspase-3 derived form of mammalian STE20-like kinase 1 (MST1)[20] or by the three major phosphatidylinositol-3-OH kinase-related kinases (PIKKs): ataxia telangiectasia mutated (ATM), ATM- and Rad-3 related (ATR), or DNA-dependent protein kinase (DNA-PK).[21–23] The activation of these PIKKs is apparently cell- and DNA-damage-type specific. Moreover, as H2AX phosphorylation is detectable in *ATM*$^{-/-}$ and *DNA-PK*$^{-/-}$ cells, it seems that there exists a functional redundancy among these PIKKs.[14] In sum, along caspase-dependent PCD, histone H2AX can be phosphorylated at Ser139 by MST1, JNK, or PIKKs.

As indicated above, the γH2AX function is a crucial event in AIF-mediated necroptosis in MEFs. However, little is known about the kinases implicated in the generation of γH2AX in this particular mode of PCD. Taking into consideration the absence of caspase-3-mediated MST1 function in necroptosis, the aim of the present paper is to analyze the potential role of JNK or the PIKKs in MNNG-induced caspase-independent necroptosis.

Results

MNNG induces necroptosis, a caspase-independent mode of PCD implicating RIP1. Treatment of MEFs with high doses of the alkylating DNA-damaging agent MNNG results in the induction of a form of programmed necrotic cell death initiated by the DNA-repair protein PARP-1.[9–11] The biochemical hallmarks of this type of PCD combine necrotic features such as lactate dehydrogenase release, ATP/NAD^+ dissipation, absence of oligonucleosomal DNA degradation, or double Annexin V/PI (propidium iodide)-positive labeling[10,24] (Figure 1a), with apoptotic features like calpain, BID, and BAX activation, mitochondrial transmembrane potential ($\Delta\Psi_m$) loss, mitochondrial release of tAIF (the calpain-cleaved form of AIF), cytochrome c, Omi/HtrA2, or Smac/DIABLO to cytosol, or TUNEL-detectable 3′-OH DNA breaks (Figures 1b–d).[9–11] Among the proapoptotic proteins released from mitochondria after MNNG treatment, AIF has a central role.[10]

The caspase independence of this type of PCD was confirmed in caspase-9 and caspase-3 gene knockout MEFs[10] and by the use of broad caspase inhibitors (Figure 1e). Additionally, we found that in comparison with *RIP*$^{+/+}$ cells, MNNG-mediated PCD was significantly inhibited in *RIP1*$^{-/-}$ MEFs. As an internal control for the RIP1 implication in MNNG-induced necroptosis, the use of the inhibitor Nec-1 also blocked this necroptotic form of PCD (Figure 1e). Moreover, by means of a new immunoblot approach, we unveiled that RIP1 is phosphorylated early after MMNG-treatment (Figure 1f). This assessment also revealed that the phosphorylation of RIP1 is maintained overtime after MNNG treatment. Taken together, our previous and present results confirm that treatment of MEFs with MNNG induces AIF and RIP1 mediated caspase-independent necroptosis.

MNNG generates double-strand breaks in DNA and phosphorylation of histone H2AX at Ser139. By producing O-methyl adducts, MNNG generates a severe damage in DNA that provokes the activation of nuclear repair proteins, such as PARP-1.[10] Moreover, histone H2AX is activated/phosphorylated after MNNG treatment, providing a mark of DSBs DNA damage: γH2AX. Indeed, a newly developed flow cytometry detection/quantification assay revealed a rapid and time-dependent H2AX phosphorylation on Ser139 (γH2AX) in MNNG-treated cells (Figure 2a). This result was further substantiated by immunofluorescence, which detected formation of γH2AX nuclear foci and quantified immunoblotting (Figures 2b and c). This triple analysis confirms that, in MNNG-induced necroptosis, the generation of γH2AX is a rapid and time-dependent process

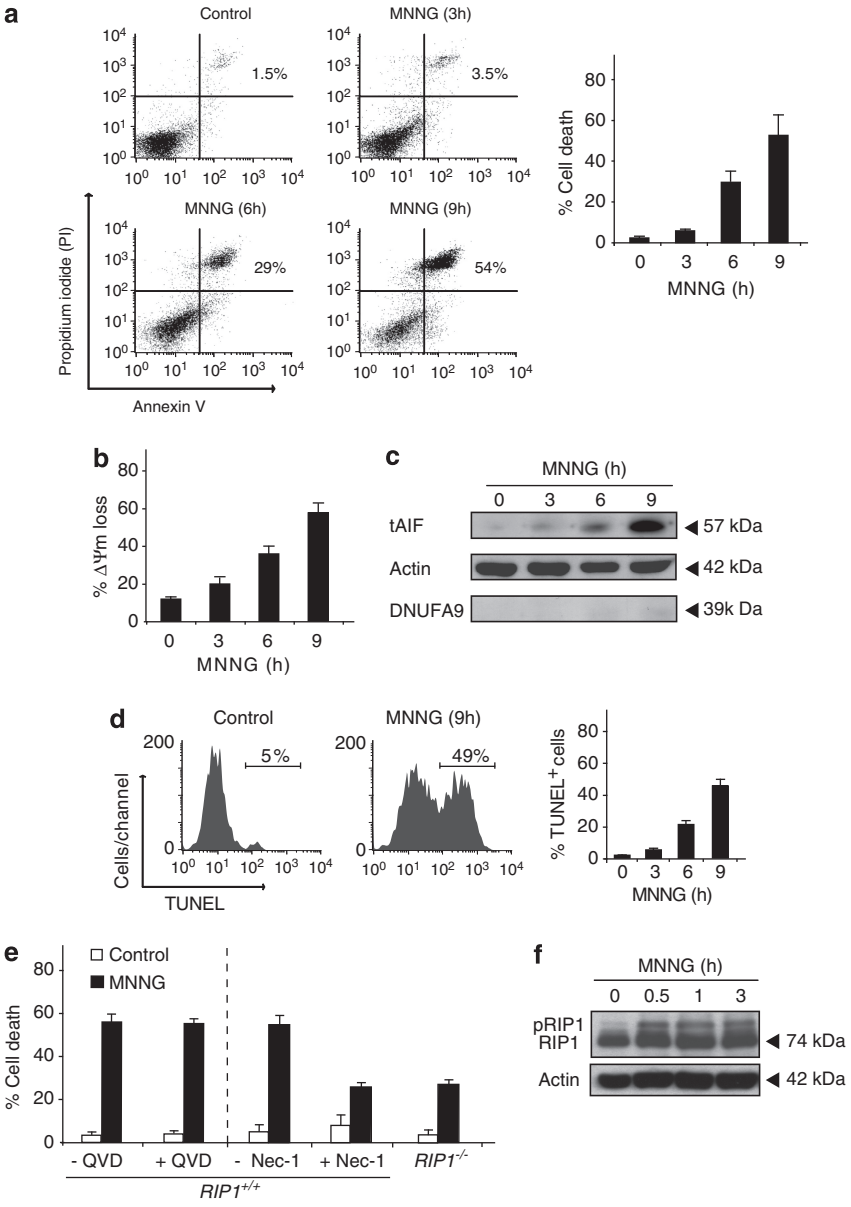

Figure 1 Biochemical characteristics of MNNG-induced necroptosis. (**a**) After the indicated time post MNNG treatment, MEFs were stained with Annexin V-APC and PI, and the frequency of double positive labeling was recorded by flow cytometry and illustrated as a plot. Data are the means of five independent experiments ± S.D. Representative cytofluorometric plots are shown. Percentages refer to Annexin V and PI double-positive staining. (**b**) Cells were treated with MNNG for the indicated times, then labeled with CMXRos, whereas the loss of the mitochondrial membrane potential ($\Delta\Psi$m) was assessed by flow cytometry and expressed as a plot. Results are the means of six independent experiments ± S.D. (**c**) Cytosolic fractions, recovered after the indicated MNNG-treatment, were blotted for tAIF detection. MNNG-treatment induces time-dependent tAIF release to cytosol. Actin (cytosolic marker) and NDUFA9 (complex I mitochondrial subunit 39) were used to control protein loading and fractionation quality. (**d**) At the indicated times post MNNG treatment, MEFs were stained for the detection of 3′-OH DNA breaks and analyzed by flow cytometry. Data are the means of six independent experiments ± S.D. In representative cytofluorometric plots, percentages refer to TUNEL-positive cells. (**e**) Assessment of cell death in *RIP*$^{+/+}$ and *RIP*$^{-/-}$ cells pre-incubated or not with the pan-caspase-inhibitor Q-VD.OPh (QVD, 10 μM) or the necroptosis inhibitor Nec-1 (10 μM) before induction of death by MNNG (9 h). Cell death was recorded by Annexin V and PI staining as in **a**. Results are the means of four independent experiments ± S.D. (**f**) RIP1 immunoblotting detection performed in WT MEFs untreated or treated with MNNG at different times. Actin was used as a loading control

detected as soon as 5 min after MNNG treatment. Note that the extent of γH2AX generated during this necroptotic process remains unchanged (even at 9 h post MNNG treatment, Figure 2c), contrary to what has been previously reported in other PCD models.[25]

The conformation of histone H2AX governs AIF-mediated necroptosis. The relevance of H2AX in AIF-mediated necroptosis has been underlined by the results indicating that *H2AX*$^{-/-}$ MEFs were less sensitive to MNNG than control cells.[11] In *H2AX*$^{-/-}$ MEFs, 9 h after MNNG treatment, the percentage of phosphatidylserine (PS) exposure and loss of viability reached $<$15%. At the same time, MNNG induced death in about 50% of *H2AX*$^{+/+}$ (WT) cells (Figures 3a and b). The lower sensitivity to MNNG displayed by *H2AX*$^{-/-}$ MEFs correlates with negative TUNEL labeling

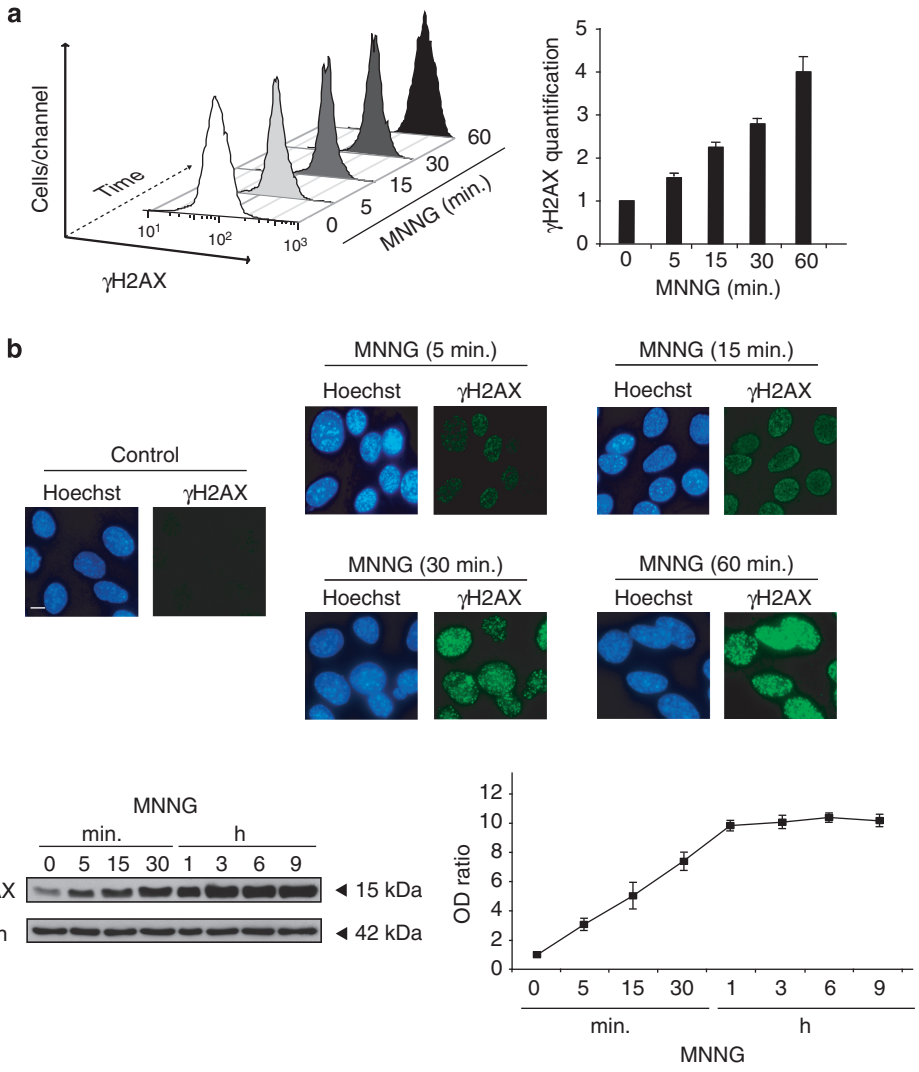

Figure 2 MNNG treatment generates DSBs in DNA and Ser139 histone H2AX phosphorylation. (**a**) Kinetics of H2AX phosphorylation induced by MNNG in MEFs. Cells were left untreated (control) or treated with MNNG at different times, and H2AX Ser139 phosphorylation was assessed by flow cytometry and expressed as a 3D plot. In the bar chart, γH2AX was quantified by the MFI and expressed as a plot. Data are mean values ± S.D. ($n = 5$). (**b**) Immunofluorescent staining of γH2AX detected in MEFs left untreated (control) or treated with MNNG at different times and stained with Hoechst 33342 (to visualize nuclei) and a γH2AX-specific antibody. Images are from a representative experiment. Bar: 10 μm. (**c**) γH2AX immunoblotting detection in total extracts obtained from MEFs untreated or treated with MNNG at different times. Actin was used to assess protein loading. The optical density ratio (OD ratio) illustrates the time course of γH2AX generation after MNNG treatment. Data are the means of four independent experiments ± S.D.

(Figure 3c). In contrast, in *H2AX*$^{-/-}$ cells, MNNG-treatment provoked mitochondrial damage as well as AIF processing and release (Figures 3d and e) in exactly the same way as in WT cells. This confirmed that the inhibition of PCD recorded in *H2AX*$^{-/-}$ MEFs is exclusively linked to the inactivation of the nuclear features characterizing MNNG-mediated necroptosis.[12] Finally, by reintroducing H2AX-wt cDNA into *H2AX*$^{-/-}$ cells by lentiviral transduction, we confirmed that the inhibition of MNNG-mediated PCD was due to the specific lack of H2AX: H2AX-wt cDNA transduction fully resensitized *H2AX*$^{-/-}$ cells to MNNG (Figures 3a–c).

H2AX phosphorylation at Ser139 during the necrotic process induced by MNNG is crucial for both the interaction of H2AX with AIF and the formation of the DNA-degrading complex that controls DNA degradation and necroptosis.[11,12] Therefore, we focused our interest on the relevance of this post-translational modification in MNNG-induced PCD. It has been previously reported that phosphorylation of H2AX at Ser139 alters H2AX conformation inside the nucleosome as well as the conformation of the nucleosome itself. These changes in H2AX/nucleosome elicit a modification in the structure and functionality of the chromatin fiber, making it accessible to diffusible factors.[14,17,26] In line with this, in MNNG-mediated PCD, transduction of *H2AX*$^{-/-}$ MEFs with a H2AX mutant that cannot be phosphorylated (H2AX-S139A, Ser139 mutated to Ala) failed to restore the ability of MNNG to induce PCD in *H2AX*$^{-/-}$ MEFs (Figures 3a–c). Surprisingly, transduction of *H2AX*$^{-/-}$ cells with an H2AX mutant that constitutively mimics the phosphorylated conformation of the protein (H2AX-S139E, with Ser139 mutated to Glu)[27] restored the responsiveness to MNNG. Thus, in the phosphorylated conformation (i.e., γH2AX or H2AX-S139E), H2AX is an active

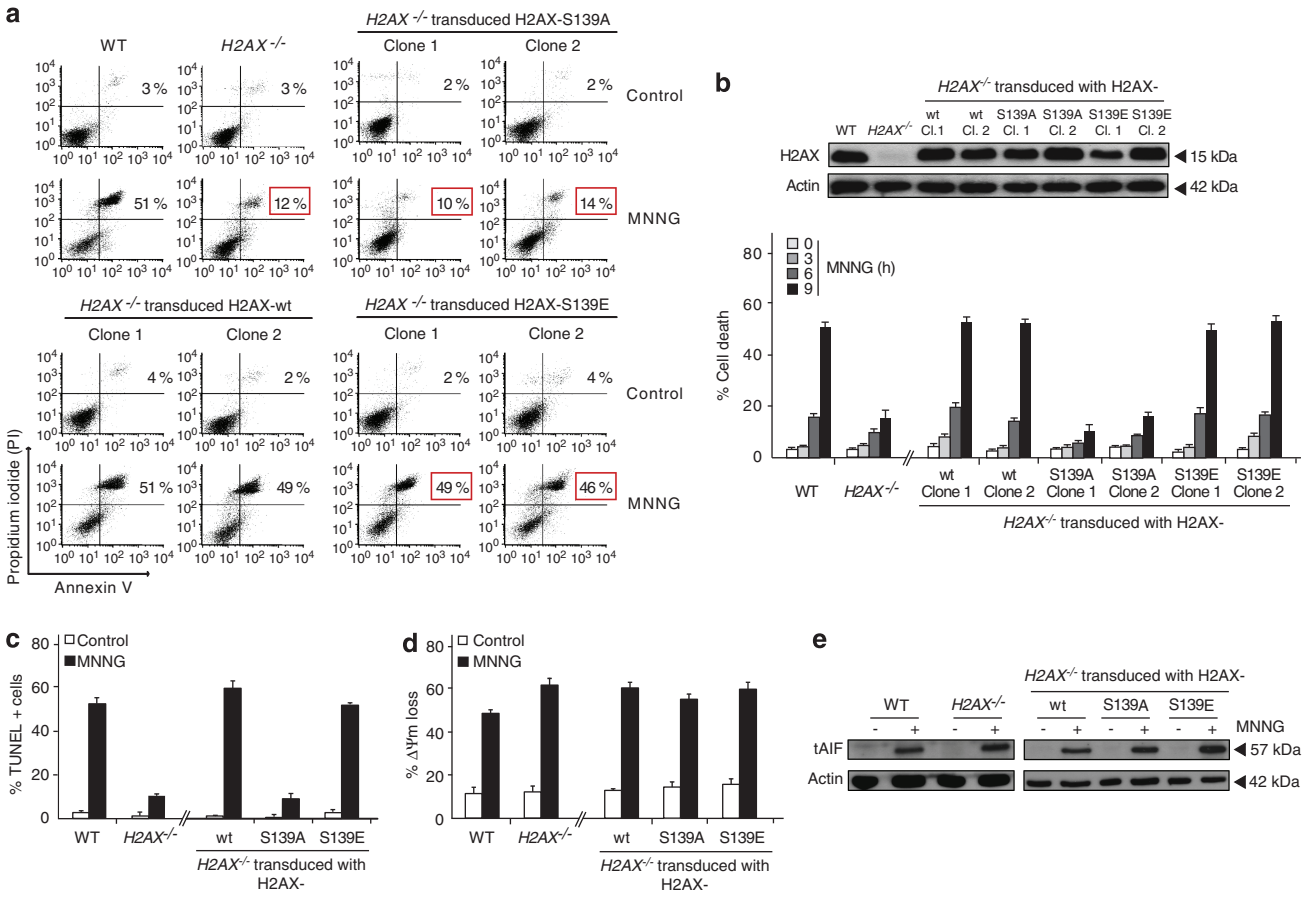

Figure 3 The phosphorylated conformation of histone H2AX governs MNNG-mediated necroptosis. (**a**) *H2AX*$^{+/+}$ (WT), *H2AX*$^{-/-}$, and two selected clones of *H2AX*$^{-/-}$ MEFs cells transduced with H2AX-wt, H2AX-S139A and H2AX-S139E cDNAs were untreated (control) or treated with MNNG (9 h), labeled with Annexin V and PI, and analyzed by flow cytometry. Representative cytofluorometric plots are shown. Percentages of cell death refer to double positive staining. Red squares highlight the high viability recorded in *H2AX*$^{-/-}$ and H2AX-S139A transduced MEFs or the loss of cell viability observed in *H2AX*$^{-/-}$ MEFs transduced with the H2AX-S139E cDNA after MNNG treatment. (**b**) Kinetic analysis of PS exposure and cell viability loss induced by MNNG in the cells described in **a**. After the indicated times, MEFs were stained with Annexin V and PI and the frequency of double positive labeling was recorded in a flow cytometer and expressed as a percentage. Data are the means of seven independent experiments ± S.D. The expression level of H2AX in these cells was assessed by immunoblotting. Equal loading was confirmed by Actin assessment. (**c**) MEFs were untreated (control) or MNNG-treated (9 h), and the presence of 3'-OH DNA breaks was assessed by flow cytometry and illustrated as a plot. Data are the means of five independent experiments ± S.D. In cytofluorometric plots, percentages correspond to TUNEL-positive cells. (**d**) MEFs described in **a** were untreated (control) or MNNG-treated (9 h), labeled with CMXRos, and assessed for $\Delta\Psi$m by flow cytometry. The frequency of cells with $\Delta\Psi$m loss was recorded and expressed as a bar chart. Data are the mean of four independent experiments ± S.D. (**e**) Cytosolic fractions recovered from the panel of MEFs used in **a** under untreated (control) or MNNG-treated (9 h) conditions were probed for tAIF detection. Actin was used to assess protein loading. Panels **c**, **d**, and **e** show the results obtained with H2AX-wt, H2AX-S139A, and H2AX-S139E in clone 1. Similar results were recorded with clone 2

necroptotic protein. On the contrary, in its non-phosphorylated conformation (i.e., H2AX-S139A), H2AX is unable to generate the DNA-degrading activity that provokes necroptosis. As for WT or *H2AX*$^{-/-}$ MEFs, MNNG-treatment provokes mitochondrial damage and AIF processing and release in H2AX-S139A and H2AX-S139E transduced cells (Figures 3d and e), confirming that the observed modulation of PCD is exclusively linked to the regulation of the nuclear features characterizing this mode of necroptosis.

Simultaneous inhibition of ATM and DNA-PK, not ATR or JNK, abolishes H2AX phosphorylation in MNNG-induced necroptosis. The critical role of the conformational state of γH2AX in caspase-independent necroptosis prompted us to investigate the kinase(s) regulating Ser139 phosphorylation. Therefore, we used a set of specific small-molecule inhibitors of ATM, ATR, DNA-PK, or JNK as a first approach to search for the kinase(s) regulating γH2AX generation. More in detail, we used KU55933 (ATMi), an ATP competitive ATM kinase inhibitor,[28] ETP-46464 (ATRi), a very recently described inhibitor of ATR,[29] NU-7026 (DNA-PKi), a highly potent DNA-PK inhibitor,[30] as well as SP-600125 (JNKi), a cell permeable JNK inhibitor.[31] All these inhibitors, used at doses described to be selective for the indicated kinase, were verified for efficiency in inhibiting the corresponding kinase phosphorylation by immunoblot or flow cytometry (Figure 4a). These approaches indicate that contrary to ATM, DNA-PK and JNK, ATR is not specifically activated/phosphorylated in our PCD model. Indeed, compared with control cells, ATR appears a bit less phosphorylated after MNNG treatment (Figure 4a). This result correlates with previously published data indicating that PARP-1, a protein highly activated in

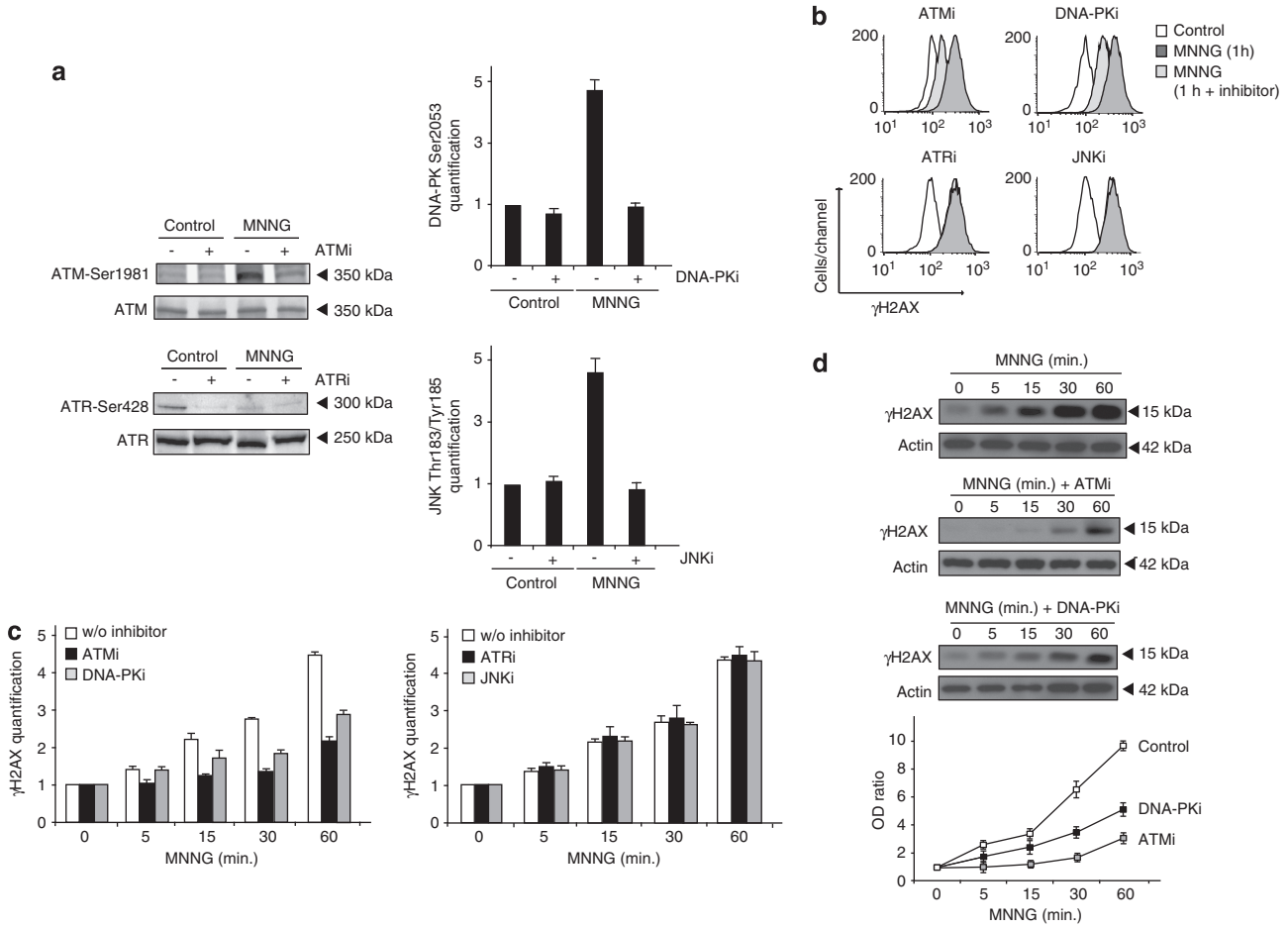

Figure 4 ATM and DNA-PK, but not JNK or ATR, modulate H2AX Ser139 phosphorylation in MNNG-induced necroptosis. (**a**) Immunoblotting or flow cytometry detection of the phosphorylated forms of ATM (Ser1981), ATR (Ser428), DNA-PK (Ser2053), and JNK (Thr183/Tyr185) obtained from MEFs untreated, treated with MNNG (1 h), or co-incubated with specific inhibitors of ATM (ATMi, 10 μM), ATR (ATRi, 15 nM), DNA-PK (DNA-PKi, 10 μM) or JNK (JNKi, 25 μM) before treatment with MNNG (1 h). See the Materials and Methods section for further details on these inhibitors. In immunoblots, total ATM or ATR were used as a loading control. (**b**) Assessment of H2AX Ser139 phosphorylation in MEFs left untreated (control), treated with MNNG (1 h), or co-incubated with the inhibitors described in **a** before treatment with MNNG (1 h). H2AX Ser139 phosphorylation was monitored by flow cytometry. Representative cytofluorometric plots are shown. (**c**) Kinetic analysis of H2AX Ser139 phosphorylation induced in MEFs treated as in **b**. After the indicated times, γH2AX was quantified as in Figure 2 and expressed as a plot. Data are the mean ± S.D. ($n = 4$). (**d**) γH2AX immunoblotting detection in total extracts obtained from MEFs untreated, treated with MNNG at different times, or co-incubated with specific inhibitors of ATM (ATMi, 10 μM) and DNA-PK (DNA-PKi, 10 μM) before treatment with MNNG. Actin was used as a loading control. The OD ratio depicted in the graph illustrates the γH2AX inhibition immunodetected in MNNG-treated MEFs co-incubated with the ATM or DNA-PK inhibitors. Data are the means of four independent experiments ± S.D.

MNNG-mediated PCD,[10] negatively regulates ATR activation/phosphorylation in MEFs.[32]

As depicted in Figure 2, MNNG-treatment induced detectable H2AX phosphorylation as soon as 5 min with a maximum of 1 h. Thus, we decided to use this timeframe in our analysis of MNNG-induced H2AX phosphorylation. It is important to underline that, in the chosen timeframe, this set of inhibitors did not provoke toxicity in MNNG-treated MEFs. After 1 h of MNNG treatment, a toxic effect precluded any kinetic assessment (data not shown). We first assessed γH2AX levels by flow cytometry. This procedure revealed that only ATM and DNA-PK inhibitors modulated MNNG-induced γH2AX generation (Figures 4b and c). On the contrary, the action of the ATR or JNK inhibitors was irrelevant in modulating Ser139-phosphorylated H2AX (Figures 4b and c). These results strongly suggest that only ATM and DNA-PK activities are implicated in the H2AX post-translational regulation. Interestingly, ATM and DNA-PK inhibitors modulate H2AX phosphorylation in a particular manner: ATMi inhibits H2AX Ser139 phosphorylation at all assessed points in time. Conversely, DNA-PKi displays a delayed modulator effect on γH2AX generation, which was first detectable only 15 min post MNNG treatment (Figure 4c). In order to substantiate our cytofluorometric data further, we carried out a complementary immunoblot assessment. As shown in Figure 4d, the immunodetection of Ser139 phosphorylated H2AX in MEFs pretreated with ATMi or DNA-PKi before MNNG addition confirms that ATM and DNA-PK regulate γH2AX production. The immunoblot quantification corroborates that ATM modulates γH2AX generation overtime and DNA-PK mediates Ser139-phosphorylated H2AX production at 15, 30, and 60 min post MNNG treatment.

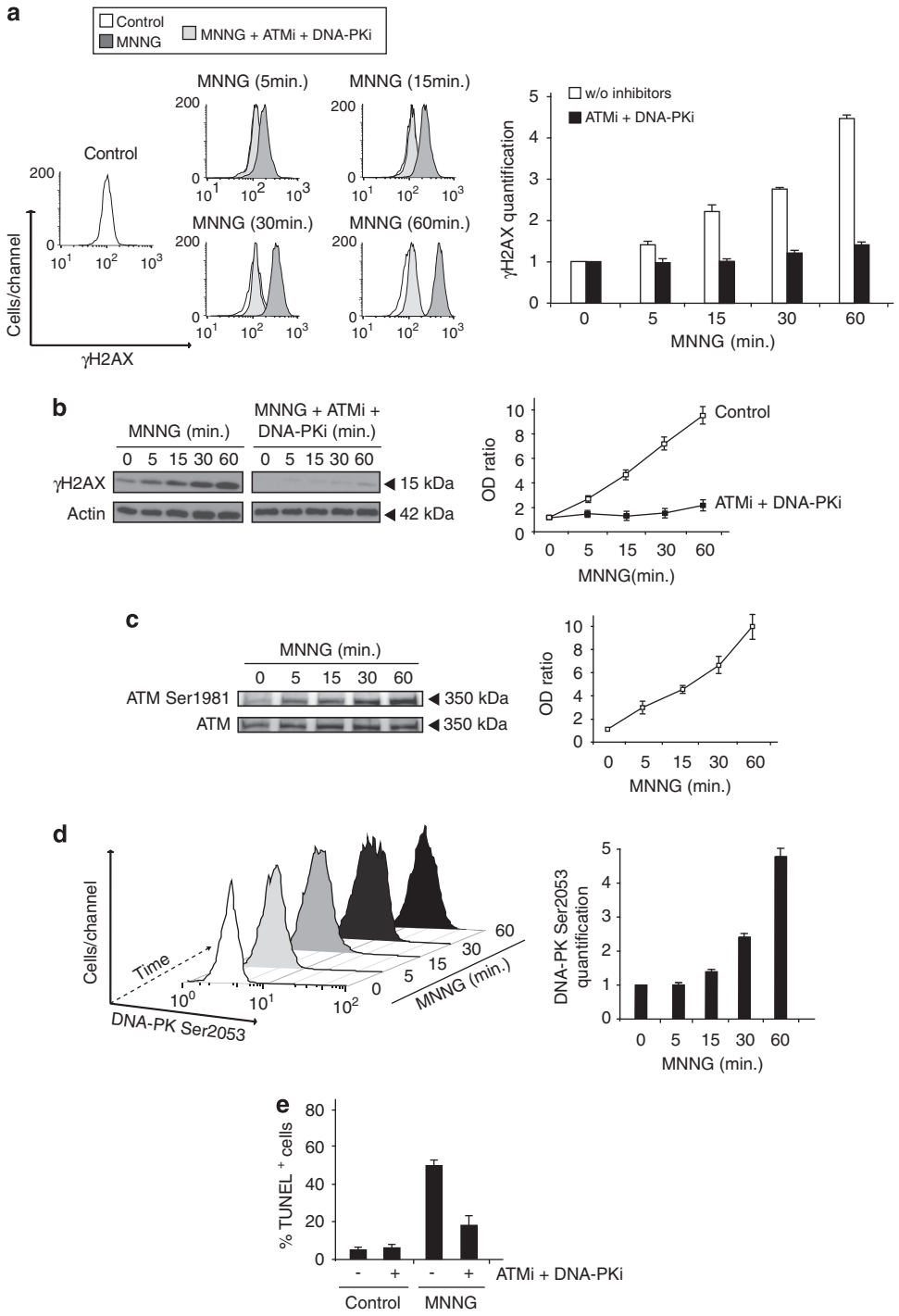

Figure 5 ATM and DNA-PK phosphorylate at Ser1981 and Ser2053, respectively, to regulate MNNG-induced γH2AX generation. (**a**) Kinetic assessment of γH2AX in MEFs left untreated (control), treated with MNNG at different times, or co-incubated with the specific inhibitors of ATM (ATMi, 10 μM) and DNA-PK (DNA-PKi, 10 μM) before treatment with MNNG. Representative cytofluorometric plots are shown. Relevant γH2AX fluorescence intensity was quantified by the MFI and expressed as a plot. Data are the means of four independent experiments ± S.D. (**b**) γH2AX immunoblotting detection in total extracts obtained from MEFs untreated, treated with MNNG at different times, or co-incubated with the inhibitors of ATM (ATMi, 10 μM) and DNA-PK (DNA-PKi, 10 μM) before treatment with MNNG. Actin was used to assess protein loading. The OD ratio in the chart depicts the γH2AX inhibition immunodetected in the presence of the ATM and DNA-PK inhibitors. Data are the mean ± S.D. ($n = 5$). (**c**) ATM Ser1981 immunoblotting detection performed in total extracts from MEFs untreated or treated with MNNG at different times. Total ATM immunodetection was used to assess protein loading. The OD ratio in the graph depicts the quantification of the relative amount of ATM Ser1981 immunodetected. Data are the means of five independent experiments ± S.D. (**d**) Kinetics of the DNA-PK Ser2053 phosphorylation induced by MNNG in MEFs. Cells were left untreated (control) or treated with MNNG at different times, and DNA-PK Ser2053 phosphorylation was assessed by flow cytometry and expressed as a 3D plot. In the bar chart, DNA-PK Ser2053 was quantified by the MFI. Data are the mean ± S.D. ($n = 4$). (**e**) MEFs untreated (control), treated with MNNG (9 h), or co-incubated with the inhibitors of ATM (ATMi, 10 μM) and DNA-PK (DNA-PKi, 10 μM) before treatment with MNNG (9 h) were stained for the detection of 3'-OH DNA breaks, analyzed by flow cytometry, and expressed as a plot. Data are the means of four independent experiments ± S.D.

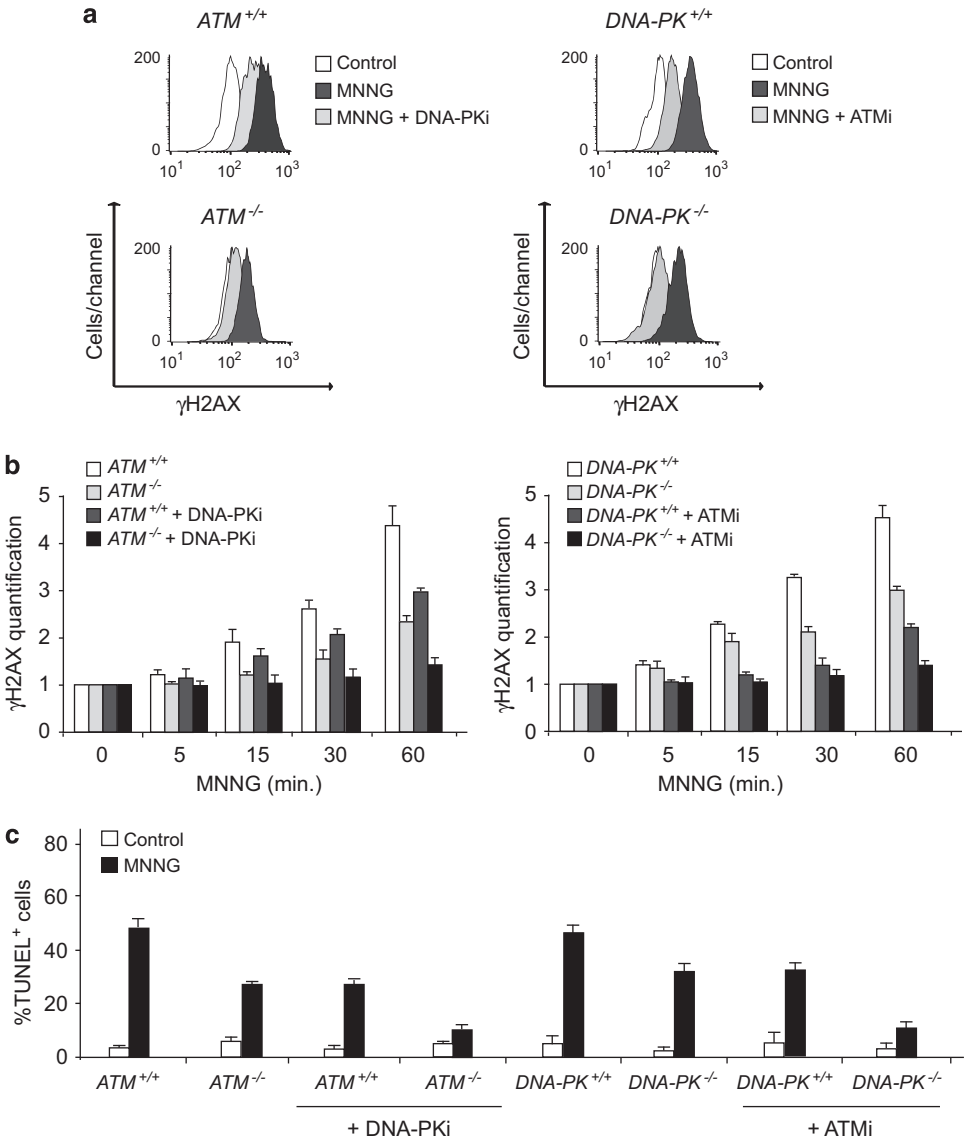

Figure 6 Genetic ablation combined with pharmacological inhibition of ATM and DNA-PK precludes MNNG-induced necroptosis. (**a**) $ATM^{+/+}$, $ATM^{-/-}$, $DNA\text{-}PK^{+/+}$, and $DNA\text{-}PK^{-/-}$ MEFs were left untreated (control), treated with MNNG (1 h), or pre-incubated with specific inhibitors of ATM (ATMi, 10 μM) and DNA-PK (DNA-PKi, 10 μM) before treatment with MNNG (1 h). H2AX Ser139 phosphorylation was recorded by flow cytometry. Representative cytofluorometric plots are shown. (**b**) Kinetic analysis of γH2AX induced in the panel of MEFs described and treated as in **a**. After the indicated times, γH2AX was quantified by the MFI and expressed as a plot. Data are mean values ± S.D. ($n = 4$). (**c**) $ATM^{+/+}$, $ATM^{-/-}$, $DNA\text{-}PK^{+/+}$, and $DNA\text{-}PK^{-/-}$ MEFs left untreated (control), treated with MNNG (9 h), or pre-incubated with the indicated inhibitor before treatment with MNNG (9 h) were stained for the detection of 3′-OH DNA breaks and analyzed by flow cytometry. Data in the bar chart are the means of four independent experiments ± S.D.

The significance of ATM and DNA-PK in MNNG-mediated PCD has also been confirmed by co-incubation of cells with inhibitors of these two PIKKs. Flow cytometry and immunoblot data demonstrate that co-incubation of $H2AX^{+/+}$ MEFs with ATMi and DNA-PKi abolishes MNNG-induced γH2AX generation (Figures 5a and b). Overall, our data reveal that ATM and DNA-PK, but not ATR or JNK, generate the Ser139-phosphorylated form of H2AX characteristic of MNNG-mediated necroptosis.

By modulating γH2AX generation, ATM and DNA-PK control MNNG-induced necroptosis. To gain insights into the impact of ATM and DNA-PK in MNNG-induced necroptosis, we analyzed the activation of these two PIKKs in further detail.[33,34] We observed that the kinetics of ATM and DNA-PK phosphorylation at Ser1981 and Ser2053 correlated with the chronological involvement of ATM and DNA-PK in MNNG-induced γH2AX generation. ATM was activated early after MNNG treatment, whereas phosphorylation of DNA-PK at Ser2053 was detectable only 15 min after DNA-damage induction (Figures 5c and d). Moreover, when pretreated with ATM and DNA-PK inhibitors, WT MEFs exhibited a significant decrease in TUNEL-detectable 3′-OH DNA breaks (Figure 5e). This indicates that the modulation of ATM and DNA-PK is sufficient not only to block γH2AX generation but also to regulate MNNG-induced necroptosis.

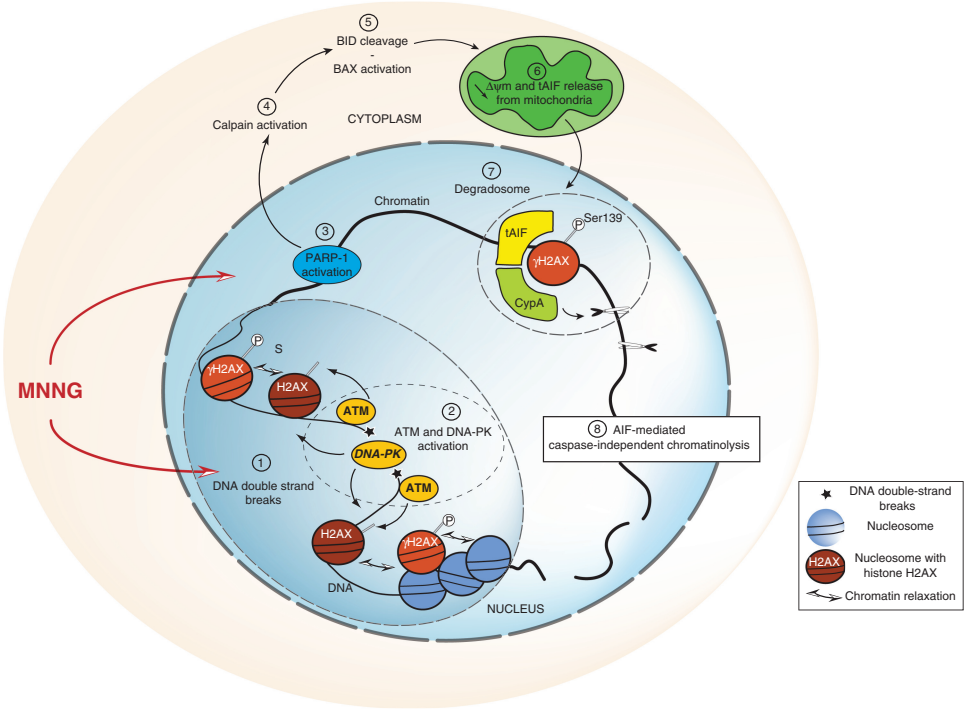

Figure 7 Representation of MNNG-induced caspase-independent necroptosis. MNNG addition generates double-strand breaks in DNA (1) and subsequent ATM/DNA-PK activation. These two PIKKs participate together in the generation of γH2AX (2). While ATM initiates histone H2AX Ser139 phosphorylation, at later steps DNA-PK seems required to maintain this phosphorylation. The DNA damage provoked in the nucleus activates the repair protein PARP-1 (3), which, through the calpain Cys proteases (4) and the BCL-2 family members BID and BAX (5), leads to the release of the necroptotic effector tAIF (truncated AIF) from the mitochondria to the cytosol (6). Upon transfer to the nucleus, tAIF associates with CypA and γH2AX to generate a DNA-degrading complex (7) that promotes AIF-mediated caspase-independent chromatinolysis (8)

The concomitant involvement of ATM and DNA-PK in MNNG-induced necroptosis was finally corroborated in *ATM*$^{-/-}$ or *DNA-PK*$^{-/-}$ MEFs treated with inhibitors of the complementary kinase. When treated with the ATM inhibitor, *DNA-PK*$^{-/-}$ cells exhibited a significant decrease in γH2AX generation and MNNG-induced chromatinolysis. Similar results were obtained in *ATM*$^{-/-}$ MEFs pretreated with a DNA-PK inhibitor (Figures 6a–c). Overall, the results obtained in gene knockout cells prove that ATM and DNA-PK have a central role in AIF-mediated caspase-independent necroptosis.

Discussion

By deciphering the signaling paths leading to the phosphorylation of histone H2AX at Ser139, the present work uncovers a new step in the mechanism regulating alkylating DNA-damage-induced necroptosis in MEFs. We indeed identified the PIKKs ATM and DNA-PK as the kinases regulating γH2AX generation in this particular mode of cell death. Combined with our previous work, our present study confirms that MNNG-mediated necroptosis is a highly regulated form of PCD involving a large network of molecular determinants: DNA-damage repair proteins, (PARP-1 and H2AX), kinases (RIP1, ATM, and DNA-PK), proteases (calpains), anti- and pro-apoptotic members of the Bcl-2 family (BID, BAX, and BCL-2), mitochondrial effectors (AIF), and DNases (CypA). So far, the involvement of all these proteins can be considered as the new signature for alkylating DNA-damage-induced caspase-independent necroptosis (Figure 7).

AIF is a main effector in the caspase-independent necroptotic process induced by the treatment of MEFs with high doses of the nitrosourea MNNG.[10] Recently, we have demonstrated that AIF promotes MNNG-mediated necroptosis via a nuclear interplay with the Ser139 phosphorylated form of histone H2AX (γH2AX).[11] Indeed, this interaction is crucial in the formation of the chromatinolytic complex that regulates necroptosis. Therefore, as AIF, γH2AX is an essential molecular determinant in MNNG-mediated necroptosis.

Initially described as inert packing material for DNA, histones regulate many cellular processes, such as gene expression, cell cycle, cell proliferation, and PCD.[35] The chromatinolytic process promoted by γH2AX is a common feature in caspase-dependent and caspase-independent PCD.[11,12,16,18,19,36] The involvement of γH2AX in PCD presents specific characteristics for these two different forms of cell death: (i) γH2AX determines the nature of the DNA degradation by regulating the accessibility of different DNases to DNA (CAD for the oligonucleosomal fragmentation associated to caspase-dependent PCD and CypA for the large-scale DNA degradation involved in caspase-independent PCD),[11,12,19] and (ii) JNK1 phosphorylates H2AX at Ser139 in UV-induced caspase-dependent PCD.[19] On the contrary, caspase-independent PCD does not require JNK for γH2AX generation (this work). Overall, all these data indicate that the same protein (H2AX) and the same post-transductional

modification (Ser139 phosphorylation) regulate different PCD pathways. This strengthens the idea that caspase-dependent and caspase-independent PCD represent alternate outcomes of a similar molecular path in which H2AX functions as a molecular switch.

A significant part of our study focuses on the relevance and consequences of the phosphorylation of H2AX on the serine 139 residue in AIF-mediated necroptosis. We first confirmed the crucial role of such phosphorylation by using a non-phosphorylatable mutant of H2AX (H2AX-S139A). However, the function of that specific post-translational modification in necroptosis still remained unexplained: it could have been either related to the recruitment of specific factors through the phosphate recognition or related to conformational changes of the nucleosome and the chromatin in general. To investigate this particular question, we used another H2AX mutant, H2AX-S139E. It has been proved that the substitution of serine in glutamate precludes phosphorylation at Ser139, but constitutively mimics the serine-phosphate structure. This mutant of H2AX has been associated with a relaxed chromatin conformation,[37] but also with an impairment of the proper maintenance of the DNA repair machinery.[27] In our model, the introduction of that phospho-mimetic mutant fully restored AIF-dependent DNA degradation and necroptosis. This confirms that AIF-mediated necroptosis requires conformational γH2AX-associated mechanisms. In this light: (i) the conformational changes caused by Ser139 H2AX phosphorylation could favor the exposure of the H2AX interface interacting with AIF. This would allow for AIF/H2AX interplay and the formation of the AIF/H2AX/CypA complex that provokes chromatinolysis and necroptosis;[11,12] (ii) In its Ser139 phosphorylated form, H2AX helps in relaxing chromatin and in maintaining its decondensed state.[38] Therefore, it seems plausible to propose that, by exposing key amino acids and by facilitating the accessibility of proteins such as AIF and CypA to DNA, the conformational modifications associated to γH2AX generation can modulate the chromatinolytic process controlling MNNG-induced necroptosis.

Our genetic and pharmacological approaches reveal that the PIKKs ATM and DNA-PK, and not other PIKKs such as ATR, regulate Ser139 H2AX phosphorylation in MNNG-induced necroptosis. We also noticed that ATM and DNA-PK act in necroptosis in a chronologically complementary manner. Indeed, ATM regulates Ser139 H2AX phosphorylation early after the DNA insult triggering necroptosis, while DNA-PK contributes further to H2AX phosphorylation (Figures 4c and d). In any case, joint action of ATM and DNA-PK is needed to generate the phosphorylated form of H2AX that controls necroptosis. This was initially revealed by a pharmacological approach: the combined action of ATM and DNA-PK inhibitors precludes γH2AX generation and PCD more efficiently than the single addition of either ATM or DNA-PK inhibitors. The coupled action of ATM and DNA-PK is further substantiated with the help of gene knockout MEFs: (i) in DNA-PK$^{-/-}$ cells, ATM inhibition prevents the γH2AX generation observed after MNNG addition and, consequently, blocks AIF-mediated chromatinolysis; (ii) in ATM$^{-/-}$ cells, DNA-PK inhibition abolishes both γH2AX generation and PCD. Therefore, it seems that the combined action of DNA-PK and ATM is required for the optimal control of alkylating DNA-damage-mediated necroptosis.

How ATM and DNA-PK are activated in MNNG-mediated necroptosis is a key question for further studies. Data obtained in other biological systems indicate that recruitment to the damage site is important for ATM activation in response to DNA damage. Controversy remains, however, regarding where the initial activation of ATM occurs in response to DSBs damage. It seems that the changes of chromatin structure initiate ATM activation.[39] In our paradigm, it may be interesting to analyze whether the changes in chromatin structure provoked by the treatment of MEFs with the nitrosourea MNNG may directly activate ATM or whether even PARP-1 may directly activate ATM, as has been suggested in other PCD programs.[40] In the case of DNA-PK, its function and activation seem related to Ku70/80-dependent localization.[39] Ku70/80 forms a complex with high affinity for DNA ends. Binding of Ku70/80 to DNA ends provides a scaffold for the association of DNA-PK. The analysis of the role of the Ku70/80 complex in necroptosis could therefore highlight the upstream signaling behind DNA-PK activation.

Post-translational modifications of proteins are considered as crucial changes in the regulation of the different cell signaling pathways. Histones, including but not limited to H2AX, are highly regulated by post-translational modifications, such as acetylation, methylation, ubiquitination, sumoylation, ADP-ribosylation, and phosphorylation.[35] Altogether, these modifications help in regulating chromatin remodeling, gene transcription, DNA repair, and PCD. Indeed, experimental evidence underpins the hypothesis of the existence of an 'apoptotic histone code' relying on H2A-ub or H2B phosphorylated on Ser14. Our results on caspase-independent necroptosis reported here now raise the question of whether there also exists a 'necroptotic histone code'. That code would be different from the apoptotic histone one, although both would imply post-translational histone modifications. A better knowledge of these codes and underlying mechanisms would certainly provide conceptual advances both in the understanding of the biology of programmed cell death and in the research of potential therapeutic targets to modulate necroptosis.

Materials and Methods

Cell culture, cell death induction and inhibition. MEFs were cultured in Dulbecco's modified Eagle's medium supplemented with 10% fetal calf serum (FCS), 2 mM L-glutamine, and 100 U/ml penicillin/streptomycin (Life Technologies, Cergy-Pontoise, France), and maintained at 37 °C in a 5% CO_2 atmosphere. *RIP1*$^{+/+}$ and *RIP1*$^{-/-}$ cells were provided by MA Kelliher (UMass Medical School, Worcester, CA, USA), *H2AX*$^{+/+}$ and *H2AX*$^{-/-}$ MEFs by A Nussenzweig (NIH, NCI, Bethesda, MD, USA), *DNA-PK*$^{+/+}$ *and DNA-PK*$^{-/-}$ by DJ Chen (University of Texas Southwestern Medical Center, Dallas, TX, USA), and *ATM*$^{+/+}$ and *ATM*$^{-/-}$ by C Sherr and M Russel (St Jude Children's Research Hospital, Memphis, TN, USA). Unless otherwise stated, WT cells refer to *H2AX*$^{+/+}$ MEFs.

To induce alkylating DNA-damage-mediated necroptosis, MEFs were treated with MNNG (500 μM, ABCR GmbH, Karlsruhe, Germany). The treating medium was replaced after 20 min of incubation by fresh medium devoid of MNNG, and cells ($\sim$80% confluence) were cultured during the indicated times. To modulate necroptosis and caspase-dependent PCD, cells were pre-incubated (1 h) with Nec-1 (10 μM), Q-VD.OPh (Gln-Val-Asp(non-Omethylated)-Oph) (QVD, 10 μM, MP Biomedicals, Illkirch, France) before MNNG-treatment.

Flow cytometry. We used Annexin V-APC (0.1 μg/ml, BD Biosciences, Le Pont-de-Claix, France) for the assessment of PS exposure, PI (0.5 μg/ml) for cell viability analysis, and MitoTracker Red (CMXRos, 20 nM, Life Technologies) for $\Delta\Psi$m quantification. Cell death was recorded in a FACSCanto II (BD Biosciences) in the total population (10 000 cells). Data, including the assessment of mean fluorescence intensity (MFI), were analyzed using FlowJo software (TreeStar, Ashland, OR, USA).

3'-OH DNA breaks (TUNEL) detection. Detection of blunt double-stranded fragments carrying a 5′-phosphate and 3′-hydroxyl group was carried out as previously described.[10]

γH2AX immunofluorescent detection. For immunofluorescent assessment, MEFs were fixed in 1% paraformaldehyde , permeabilized with methanol/acetone (1 : 1 v/v, 10 min), incubated with an anti-γH2AX (clone JBW301, Millipore, Molsheim, France), and detected by anti-mouse IgG conjugated with Alexa Fluor 488 (Life Technologies). Fluorescence was observed in a Nikon Eclipse TE2000-U microscope and analyzed using the Nikon NIS-Elements BR software. To visualize nuclei, cells were co-stained with Hoechst 33342.

γH2AX pharmacological modulation. Before MNNG-treatment, MEFs were pre-incubated during 30 min with the following small-molecule inhibitors: 2-(4-morpholinyl)-6-(1-thianthrenyl?)-4*H*-pyran-4-one (KU-55933, ATMi, 10 μM), ethyl 6-bromo-4-chloroquinoline-3-carboxylate (ETP-46464, ATRi, 15 nM), 2-(4-morpholinyl)-4*H*-naphthol(1,2-*b*)pyran-4-one (NU-7026, DNA-PKi, 10 μM), or anthra(1,9-*cd*)pyrazol-6(2*H*)one, 1,9-pyrazoloanthrone (SP-600125, JNKi, 25 μM). KU-55933, NU-7026, and SP-600125 were from Calbiochem (San Diego, CA, USA). ETP-46464 was kindly provided by Dr. O Fernandez-Capetillo (CNIO, Madrid).

γH2AX, DNA-PK Ser2053 and JNK Thr183/Tyr185 flow cytometry assessment. At different times after MNNG treatment, 5×10^5 cells were fixed in 70% ethanol (4 °C, 2 h) and permeabilized in 0.3% Triton X-100 (10 min, RT). After centrifugation (1500 *g*, 15 min), cells were saturated in phosphate-buffered saline 0.1% Triton X-100 10% FCS (30 min, RT), incubated 1 h with anti-γH2AX, anti-DNA-PK-Ser2053 (Abcam, Paris, France) or anti-JNK-Thr183/Tyr185 (clone G9, Cell Signaling, Danvers, MA, USA), and detected by an anti-mouse or anti-rabbit IgG conjugated with Alexa Fluor 488 or 647. Data were recorded in a FACSCanto II in total cell population. γH2AX and DNA-PK-Ser2053 were quantified by the MFI of each sample and were expressed relative to the MFI obtained in untreated cells ($=1.0$).

Protein extraction, cell fractionation, and immunoblotting. 2×10^6 cells were washed twice with ice-cold phosphate-buffered saline containing 5 mM Na-orthovanadate and 50 mM sodium fluoride. Total protein extraction was performed by sonication in buffer containing 10 mM HEPES (pH 7.5), 5 mM KCl, 2.5 mM EDTA, 0.5 mM DTT, 2.5 mM PMSF, 5 mM iodoacetamide and 0.5% Nonidet P-40. Histones were purified after lysis of 1×10^6 cells in NETN buffer (150 mM NaCl, 1 mM EDTA, 20 mM Tris (pH 8) and 0.5% Nonidet P-40), centrifuged (16 000 *g*, 5 min, 4 °C) followed by resuspension of the pellet in acidic solution (0.1 M HCl).[19]

For cytosolic extracts, MEFs were resuspended in buffer containing 220 mM mannitol, 70 mM sucrose, 50 mM Hepes-KOH (pH 7.2), 10 mM KCl, 5 mM EGTA, 2 mM $MgCl_2$, and 0.025% digitonin, and kept on ice for 5 min. Lysed cells were centrifuged (16 000 *g*, 5 min, 4 °C) and the supernatant was retained as cytosolic fraction. Protein concentration was determined using the BioRad Protein Assay. Equal amounts of total proteins (40 to 150 μg) were loaded on linear SDS-PAGE gels and transferred onto a nitrocellulose membrane. Membrane blocking and antibody incubations were performed in phosphate-buffered saline 0.1% Tween 20 plus 5% non-fat dry milk.

Membranes were probed with primary antibodies against H2AX, γH2AX (Millipore), RIP1/phospho RIP1 (BD Biosciences, clone 38/RIP), ATM (clone 2C1, GeneTex, Irvine, CA, USA), ATM-Ser1981 (this Ab also recognizes Ser1987 in mouse, clone 10H11.E12, Rockland, Gilbertsville, PA, USA), ATR, ATR-Ser428 (Cell Signaling), AIF, mitochondrial complex I NDUFA9 (Life Technologies, clone 20C11), and β-actin (clone AC-15). Immunoreactive proteins were detected using HRP-conjugated secondary antibodies and revealed by the ECL system. Immunoblot images were acquired in a Bio-Imaging System MF-ChemiBis 4.2 (DNR Bio-Imaging Systems, Jerusalem, Israel) or in a Kodak X-OMAT 1000 processor (Kodak, Chalon-sur-Saone, France).

γH2AX and ATM-Ser1981 were quantified using the Multi Gauge 3.0 software (Fujifilm Life Sciences, Bois d'Arcy, France). The optical density was normalized according to an endogenous background and was expressed relative to the data obtained in untreated cells ($=1.0$).

Vectors and lentiviral transduction. H2AX-wt, H2AX-S139A, and H2AX-S139E cDNAs were cloned into the pLVX-IRES-Zs-Green lentiviral vector (Clontech-Takara Bio Europe, Saint-Germain-en-Laye, France). Viruses were produced into 293T cells by $CaCl_2$ transient transfection of the lentiviral constructs and the packaging plasmids pMD2.G and psPAX-2 (Addgene plasmids 12259 and 12260, respectively). Forty-eight hours after transfection, lentiviral supernatants were harvested, clarified by filtration, and used immediately for *H2AX*$^{-/-}$ MEFs transduction with 4 μg/ml of polybrene. Seventy-two hours after transduction, cells were diluted for immunoblot selection of individual clones. Clones with similar H2AX levels to *H2AX*$^{+/+}$ MEFs were selected, expanded, and analyzed.

Unless specified, chemicals and reagents were from Sigma-Aldrich.

Conflict of Interest

The authors declare no conflict of interest.

Acknowledgements. We are grateful to Drs. A Nussenzweig, DJ Chen, CJ Sherr, M Russel, and MA Kelliher for immortalized MEFs, NV Tomilin (Institute of Cytology, St. Petersburg) for H2AX, H2AXS139A, and H2AXS139E cDNAs, O Fernandez-Capetillo and M Murga (CNIO, Madrid) for the ATR inhibitor ETP-46464, and S Krantic and M Segade for critical reading of the paper. This work was supported by Agence Nationale de la Recherche (contract ANR-09-BLAN-0247), Ligue Contre le Cancer (Comités de Paris et du Val d'Oise), Fondation ARC (contract 5104), Association Laurette Fugain, and Fondation de France (to SA Susin). M Baritaud and L Cabon receive PhD fellowships from Ministère de l'Enseignement Supérieur et de la Recherche and Ecole Normale Supérieure-Cachan, respectively.

1. Vandenabeele P, Galluzzi L, Vanden Berghe T, Kroemer G. Molecular mechanisms of necroptosis: an ordered cellular explosion. *Nat Rev Mol Cell Biol* 2010; **11**: 700–714.
2. Yuan J, Kroemer G. Alternative cell death mechanisms in development and beyond. *Genes Dev* 2010; **24**: 2592–2602.
3. Vanlangenakker N, Vanden Berghe T, Vandenabeele P. Many stimuli pull the necrotic trigger, an overview. *Cell Death Differ* 2012; **19**: 75–86.
4. Degterev A, Hitomi J, Germscheid M, Ch'en IL, Korkina O, Teng X *et al.* Identification of RIP1 kinase as a specific cellular target of necrostatins. *Nat Chem Biol* 2008; **4**: 313–321.
5. Sun L, Wang H, Wang Z, He S, Chen S, Liao D *et al.* Mixed lineage kinase domain-like protein mediates necrosis signaling downstream of RIP3 kinase. *Cell* 2012; **148**: 213–227.
6. Wang Z, Jiang H, Chen S, Du F, Wang X. The mitochondrial phosphatase PGAM5 functions at the convergence point of multiple necrotic death pathways. *Cell* 2012; **148**: 228–243.
7. Delavallee L, Cabon L, Galan-Malo P, Lorenzo HK, Susin SA. AIF-mediated caspase-independent necroptosis: a new chance for targeted therapeutics. *IUBMB Life* 2011; **63**: 221–232.
8. Xu Y, Huang S, Liu ZG, Han J. Poly(ADP-ribose) polymerase-1 signaling to mitochondria in necrotic cell death requires RIP1/TRAF2-mediated JNK1 activation. *J Biol Chem* 2006; **281**: 8788–8795.
9. Cabon L, Galan-Malo P, Bouharrour A, Delavallee L, Brunelle-Navas MN, Lorenzo HK *et al.* BID regulates AIF-mediated caspase-independent necroptosis by promoting BAX activation. *Cell Death Differ* 2012; **19**: 245–256.
10. Moubarak RS, Yuste VJ, Artus C, Bouharrour A, Greer PA, Menissier-de Murcia J *et al.* Sequential activation of poly(ADP-Ribose) polymerase 1, Calpains, and Bax is essential in apoptosis-inducing factor-mediated programmed necrosis. *Mol Cell Biol* 2007; **27**: 4844–4862.
11. Artus C, Boujrad H, Bouharrour A, Brunelle MN, Hoos S, Yuste VJ *et al.* AIF promotes chromatinolysis and caspase-independent programmed necrosis by interacting with histone H2AX. *EMBO J* 2010; **29**: 1585–1599.
12. Baritaud M, Boujrad H, Lorenzo HK, Krantic S, Susin SA. Histone H2AX: The missing link in AIF-mediated caspase-independent programmed necrosis. *Cell Cycle* 2010; **9**: 3166–3173.
13. Yuste VJ, Moubarak RS, Delettre C, Bras M, Sancho P, Robert N *et al.* Cysteine protease inhibition prevents mitochondrial apoptosis-inducing factor (AIF) release. *Cell Death Differ* 2005; **12**: 1445–1448.
14. Fernandez-Capetillo O, Lee A, Nussenzweig M, Nussenzweig A. H2AX: the histone guardian of the genome. *DNA Repair (Amst)* 2004; **3**: 959–967.
15. Rogakou EP, Pilch DR, Orr AH, Ivanova VS, Bonner WM. DNA double-stranded breaks induce histone H2AX phosphorylation on serine 139. *J Biol Chem* 1998; **273**: 5858–5868.
16. Bonner WM, Redon CE, Dickey JS, Nakamura AJ, Sedelnikova OA, Solier S *et al.* GammaH2AX and cancer. *Nat Rev Cancer* 2008; **8**: 957–967.

17. Fernandez-Capetillo O, Celeste A, Nussenzweig A. Focusing on foci: H2AX and the recruitment of DNA-damage response factors. *Cell Cycle* 2003; **2**: 426–427.
18. Rogakou EP, Nieves-Neira W, Boon C, Pommier Y, Bonner WM. Initiation of DNA fragmentation during apoptosis induces phosphorylation of H2AX histone at serine 139. *J Biol Chem* 2000; **275**: 9390–9395.
19. Lu C, Zhu F, Cho YY, Tang F, Zykova T, Ma WY *et al.* Cell apoptosis: requirement of H2AX in DNA ladder formation, but not for the activation of caspase-3. *Mol Cell* 2006; **23**: 121–32.
20. Wen W, Zhu F, Zhang J, Keum YS, Zykova T, Yao K *et al.* MST1 promotes apoptosis through phosphorylation of histone H2AX. *J Biol Chem* 2011; **285**: 39108–39116.
21. Burma S, Chen BP, Murphy M, Kurimasa A, Chen DJ. ATM phosphorylates histone H2AX in response to DNA double-strand breaks. *J Biol Chem* 2001; **276**: 42462–42467.
22. Mukherjee B, Kessinger C, Kobayashi J, Chen BP, Chen DJ, Chatterjee A *et al.* DNA-PK phosphorylates histone H2AX during apoptotic DNA fragmentation in mammalian cells. *DNA Repair (Amst)* 2006; **5**: 575–590.
23. Ward IM, Chen J. Histone H2AX is phosphorylated in an ATR-dependent manner in response to replicational stress. *J Biol Chem* 2001; **276**: 47759–47762.
24. Boujrad H, Gubkina O, Robert N, Krantic S, Susin SA. AIF-mediated programmed necrosis: a highly regulated way to die. *Cell Cycle* 2007; **6**: 2612–2619.
25. Rogakou EP, Boon C, Redon C, Bonner WM. Megabase chromatin domains involved in DNA double-strand breaks *in vivo*. *J Cell Biol* 1999; **146**: 905–916.
26. Thiriet C, Hayes JJ. Chromatin in need of a fix: phosphorylation of H2AX connects chromatin to DNA repair. *Mol Cell* 2005; **18**: 617–622.
27. Celeste A, Difilippantonio S, Difilippantonio MJ, Fernandez-Capetillo O, Pilch DR, Sedelnikova OA *et al.* H2AX haploinsufficiency modifies genomic stability and tumor susceptibility. *Cell* 2003; **114**: 371–383.
28. Hickson I, Zhao Y, Richardson CJ, Green SJ, Martin NM, Orr AI *et al.* Identification and characterization of a novel and specific inhibitor of the ataxia-telangiectasia mutated kinase ATM. *Cancer Res* 2004; **64**: 9152–9159.
29. Toledo LI, Murga M, Zur R, Soria R, Rodriguez A, Martinez S *et al.* A cell-based screen identifies ATR inhibitors with synthetic lethal properties for cancer-associated mutations. *Nat Struct Mol Biol* 2011; **18**: 721–727.
30. Veuger SJ, Curtin NJ, Richardson CJ, Smith GC, Durkacz BW. Radiosensitization and DNA repair inhibition by the combined use of novel inhibitors of DNA-dependent protein kinase and poly(ADP-ribose) polymerase-1. *Cancer Res* 2003; **63**: 6008–6015.
31. Bennett BL, Sasaki DT, Murray BW, O'Leary EC, Sakata ST, Xu W *et al.* SP600125, an anthrapyrazolone inhibitor of Jun N-terminal kinase. *Proc Natl Acad Sci USA* 2001; **98**: 13681–13686.
32. Kedar PS, Stefanick DF, Horton JK, Wilson SH. Interaction between PARP-1 and ATR in mouse fibroblasts is blocked by PARP inhibition. *DNA Repair (Amst)* 2008; **7**: 1787–1798.
33. Bakkenist CJ, Kastan MB. DNA damage activates ATM through intermolecular autophosphorylation and dimer dissociation. *Nature* 2003; **421**: 499–506.
34. Chen BP, Chan DW, Kobayashi J, Burma S, Asaithamby A, Morotomi-Yano K *et al.* Cell cycle dependence of DNA-dependent protein kinase phosphorylation in response to DNA double strand breaks. *J Biol Chem* 2005; **280**: 14709–14715.
35. Strahl BD, Allis CD. The language of covalent histone modifications. *Nature* 2000; **403**: 41–45.
36. Solier S, Sordet O, Kohn KW, Pommier Y. Death receptor-induced activation of the Chk2- and histone H2AX-associated DNA damage response pathways. *Mol Cell Biol* 2009; **29**: 68–82.
37. Downs JA, Lowndes NF, Jackson SP. A role for saccharomyces cerevisiae histone H2A in DNA repair. *Nature* 2000; **408**: 1001–1004.
38. Kruhlak MJ, Celeste A, Dellaire G, Fernandez-Capetillo O, Muller WG, McNally JG *et al.* Changes in chromatin structure and mobility in living cells at sites of DNA double-strand breaks. *J Cell Biol* 2006; **172**: 823–834.
39. Lovejoy CA, Cortez D. Common mechanisms of PIKK regulation. *DNA Repair (Amst)* 2009; **8**: 1004–1008.
40. Haince JF, Kozlov S, Dawson VL, Dawson TM, Hendzel MJ, Lavin MF *et al.* Ataxia telangiectasia mutated (ATM) signaling network is modulated by a novel poly(ADP-ribose)-dependent pathway in the early response to DNA-damaging agents. *J Biol Chem* 2007; **282**: 16441–16453.